# Modelling, simulation and experimental verification for Renewable agents connected to a distorted utility grid using a Real-Time Digital Simulation Platform

N. F. Guerrero-Rodríguez[a*], Alexis B. Rey-Boué[b]

[a*] Department of Electronics, Computers Technology and Projects, Universidad Politécnica de Cartagena, c/Dr. Fleming, s/n 30202, Cartagena, Murcia, Spain. Tel.: +34 968 326514; fax: +34 968 326400, E-mail address: nestor.guerrero@upct.es

[b] Department of Electronics, Computers Technology and Projects, Universidad Politécnica de Cartagena, c/Dr. Fleming, s/n 30202, Cartagena, Murcia, Spain. Tel.: +34 968 325928; fax: +34 968 326400, E-mail address: alexis.rey@upct.es

*Corresponding autor: N. F. Guerrero-Rodríguez

## Abstract

The large number of Photovoltaic plants and its utilization as agents of a Distributed Generation Systems justified the increasing efforts towards the optimal design of the overall grid-connected System. In a Distributed Generation environment the low voltage 3-phase utility grid could be affected by some disturbances such as voltage unbalanced, variations of frequency and harmonics distortion and it is mandatory that the control algorithms used in the inverter can be able to maintain the power flow between the renewable agent and the low voltage 3-phase utility grid; in addition a unitary power factor must be attained.

A Proportional-Resonant regulator is used to performance a current control with the output current of the inverter and a Multiple Second Order Generalized Integrator Frequency-Locked Loop (MSOGI-FLL) is used to detect the frequency of the low voltage 3-phase utility grid. Some low order harmonics are introduced in the low voltage 3-phase utility grid in order to see the effect of the harmonic compensator.

In order to validate the model of the Photovoltaic Renewable agent, the synchronization algorithm and the inverter control algorithm, some simulations using MATLAB/SIMULINK from The MathWorks, Inc. are shown firstly, and secondly, some Real-Time Digital Simulation tests using the a Real-Time Digital Simulation (RTDS) platform are carried out.

**Keywords:** Photovoltaic Generator, Real-Time Digital Simulation, harmonic-compensator, MSOGI-FLL, Proportional-Resonant regulator.

## 1. Introduction

Fossil fuels have been the primary energy source for decades, playing the key role in the Power Generation Systems have been the primary energy source for decades, playing the key role in the Power Generation Systems. However, its reserves are to be extinguished in a near future, and the Industrial Plants involving them have contributed negatively to the pollution of the environment because of $CO_2$ emissions and, consequently, the greenhouse effect and the depletion of the ozone layer; on the other hand, the price have increased continuously during the recent years, allowing people and governments to realize that it is not a good policy to be fuel-depending. In order to mitigate this negative tendency, several International Organizations and Committees have established limitations in the emissions that countries and regions in the world can produced [1] and many European governments have decided to promote the use of Renewable Energies as an emerging clean alternative for the generation of electricity [2]. In this way, the recent liberalization of the European electrical market has led to the forthcoming of many dispersed Renewable generation systems [3], such as Photovoltaic Generators (PV Generators) [4], working as agents in Distributed Generation Systems (DG).

In PV grid-connected facilities, the PV Generator is connected through an inverter which supplies the incoming energy directly to the utility grid [3]. Usually, the inverters used in PV applications implement a Maximum Power Point Tracking (MPPT) algorithm in order to extract the maximum available power from the PV Generator for specific irradiance and temperature conditions [5]. For 3-phase systems, it is a most to exert a decoupled control of the active and reactive power of the inverter-grid connection, and several current control algorithms, such as hysteresis control [6], and d-q control [7] can be used for deciding the state of the power-poles.

The low voltage 3-phase utility grid is affected by some of the following perturbations: grid voltage unbalances which produce second order harmonics in the dc voltage bus [8], variations of its nominal frequency that may lead to the power factor degradation of the inverter-grid connection, and low order harmonics produced by non-linear loads. So, new and sophisticated synchronization and control algorithms must be designed in order to attain a reliable detection of the phase and the frequency of the utility grid, as well as to control properly the line currents of the inverter, respectively, both in the presence of these disturbances. When the low order frequency harmonics ($5^{th}$, $7^{th}$, $11^{th}$, $13^{th}$, $17^{th}$, $19^{th}$, etc.=$6n\pm1$, $n=1,2,3,\ldots$) distortions perturb the utility grid voltage, the controlled line currents of the inverter will also be distorted as well, reducing the power quality of the inverter-grid connection, unless a harmonic compensation strategy were used.

In [9] [10], a Voltage Source Inverter (VSI) working as a shunt active filter is proposed as a harmonic compensator scheme at the point of common coupling (PCC) of the distribution 3-phase line voltages and nonlinear loads: in this, the 3-phase line currents of the inverter are controlled in the Synchronous Reference frame (SRF) (abc->dq transformation needed) so as to feed 3-phase “pure” sinusoidal currents into the utility grid; however, this type of harmonic compensator behaves as a feedforward open-loop control which is affected, essentially, by the line currents control delay and the harmonic cancellation cannot be done completely. If some low-pass filter, with a cutoff frequency that produces a leading phase equal to the currents delay, is employed to

sense the currents, the delay effect can be reduced [11]. The same idea is exposed in [12], where a Stationary Reference frame approach is used.

In order to overcome the effect of the delay effect, a closed-loop harmonic compensation (HC) structure in the SRF is described in [11], allowing a total compensation of selected harmonic currents. However, this approach involves an extremely complex structure needed for the positive and negative sequence of each harmonic to be compensated and, consequently, a high computational burden is required, unless the control of the 3-phase currents and the harmonic compensation were exerted in the Stationary Reference frame (abc->αβ transformation needed) [13]. The latter will be explained in this article.

In this paper, a 10kW PV grid-connected (three wire configuration) PV agent will be modelled and described by means of the control and power subsystems, and the effect of the harmonic pollution will be studied as well. For this, the $5^{th}$ and $7^{th}$ harmonics will be introduced in the 3-phase utility grid voltages because they are relatively closed to its fundamental frequency (50Hz) and its contribution to the harmonic distortions in the controlled currents to be fed into the utility grid is more remarkable, although the attained results can be extended to the rest of low order harmonics (the zero-sequences of the multiple of the third harmonics are not considered because they have no effect due to the three wire configuration employed). Moreover, the several normatives [14,15] are indeed more restrictive in the allowed distortion of grid currents for lower order harmonics.

With the purpose to obtain a grid-connected PV renewable agent capable to operate efficiently when high level of voltage harmonic pollutions occur, several algorithms are combined in this paper in order to obtain a control system able to maintain the proper operation of the renewable agent which fulfills the power quality standards: the control of the Voltage Source Inverter (VSI) will include a Multiple Second Order Generalized Integrator Frequency-Locked Loop (MSOGI-FLL) structure [16] as the synchronization algorithm, a conventional Proportional-Integral (PI) regulator for the outer dc bus voltage, a Proportional-Resonant (PR) regulator [8,17] for the control of the inner currents, and a Harmonic Compensator (HC) [8] structure so as to improve the quality of the power injected to the utility grid, yielding a grid-connected PV system insensitive to harmonic pollution.

The performance of the grid-connected PV agents will be studied with several simulations using MATLAB/SIMULINK tool [18], when unbalances in the 3-phase utility grid voltages, harmonic distortions and frequency variations occur. Real-time digital simulations of the Power and Control Subsystems will be performed using a DS1006 DSPACE platform in order to reinforce the validity of the preliminary results. Finally, some conclusions are shown.

## 2. Power and Control Subsystems

The Power and Control Subsystems of the involved PV Generator together with a 3-phase inverter-grid-connected system are depicted in Fig. 1. The Power Subsystem is at the upper side and the Control Subsystem is at the lower side.

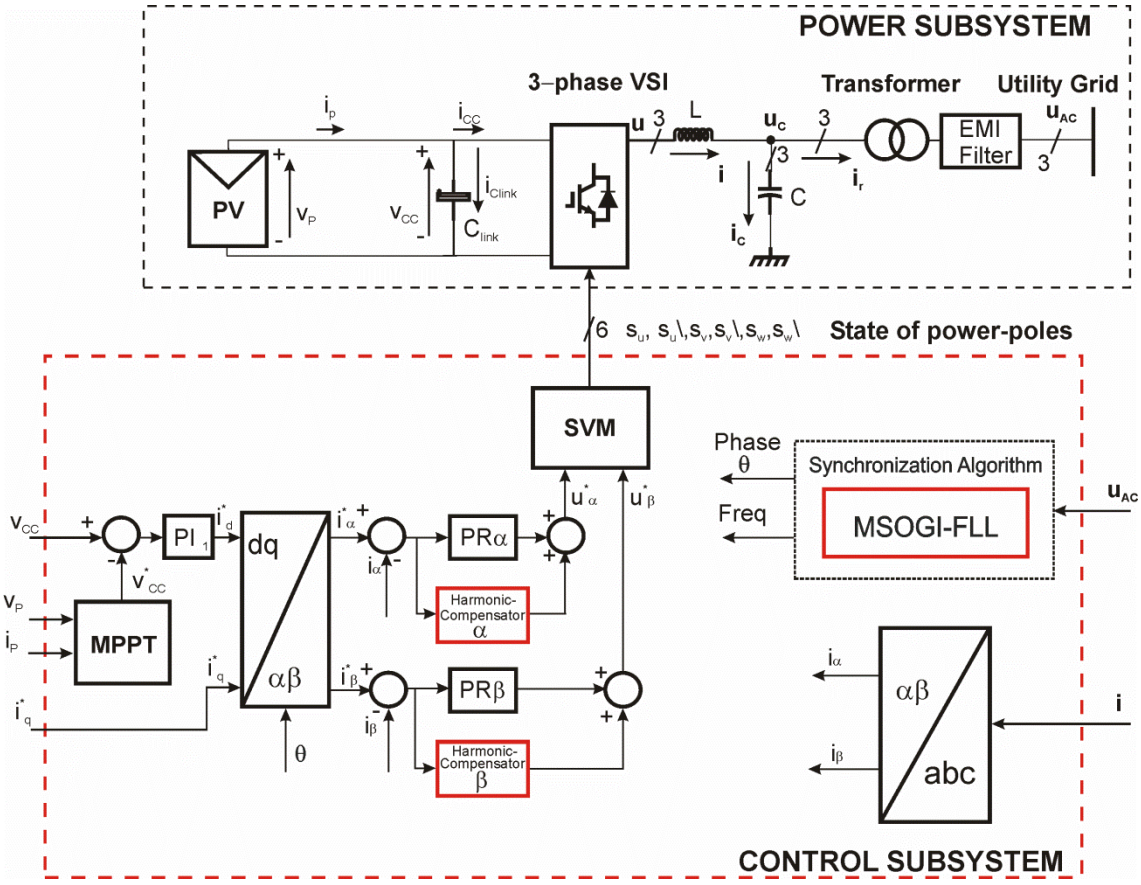


**Fig. 1.** Block diagram of the Power and Control Subsystems for a 3-phase grid-connected system (the ac side in the Power Subsystem is represented by its equivalent 1-phase circuit for simplicity).

### *2.1 Power Subsystem*

The power subsystem is formed by:

#### *2.1.1 Photovoltaic modules:*

PV modules are the main part of a PV system [19]. There are several kinds of PV modules technologies with different levels of efficiencies. The function of a PV module is to supply the necessary power for the renewable grid-connected system, which will be a function of the available solar irradiance. The size (arrange of parallel-series PV cells) of the PV module will be a function of the required power of the Photovoltaic system. Interested readers may find some additional information in the scientific literature, such as [20-22]

#### *2.1.2 The inverter:*

The mission of the inverter is to convert the generated dc voltage into suitable ac currents to be fed into the 3-phase low-voltage utility grid [3]. The inverter is mainly built with semi-conductor electronic devices (IGBTs and Diodes). The Space Vector Modulation technique (SVM) [23] is used to control the trigger of the power switches according to the averages of the voltages and currents references, although the Pulse-

Width Modulation (PMW) technique can be used instead. According to Fig. 1, the dc side of the inverter can be described as follows:

Applying the Kirchhoff's current law to the input node yields:

$$i_p = i_{clink} + i_{CC} \tag{1}$$
$$i_{CC} = s_u \cdot i_u + s_v \cdot i_v + s_w \cdot i_w$$
$$i_{clink} = C_{link} \frac{dv_{CC}}{dt}$$
$$P_{PV} = i_p v_p$$

where $v_p$, $i_p$ are the voltage and the output current of the PV generator, respectively, $P_{PV}$ is the available power for a specific irradiance, $v_{CC}$ is the dc bus voltage, $i_{clink}$ is the current through the link capacitor $C_{link}$, and $i_{CC}$ is the current delivered to the 3-phase VSI (which is a function of the line currents $i_u, i_v, i_w$ and the states of the power-poles $s_u, s_v, s_w$ (1:'on', 0:'off', $s_i$-upper pole, $s_i$\-lower pole in the 3-phase VSI).

Assuming that the voltages in the capacitors of the LCL branch are approximately the same as the voltages in the utility grid, the dynamic at the output of the 3-phase VSI can be described by the following vector equation [24]:

$$\mathbf{u} - \mathbf{u_{AC}} = R\mathbf{i} + L\frac{d\mathbf{i}}{dt} = \mathbf{u_R} + \mathbf{u_L} \tag{2}$$

where **u** is the inverter voltage vector, **i** is the inverter line current vector, $\mathbf{u_{AC}}$ is the utility grid voltage vector, L is the line inductance, and R is its resistance.

Neglecting the losses of the distribution transformer and the EMI filter and expressing the last vector equation with its $\alpha\beta$ components [13], the power flow between the 3-phase VSI and the utility grid can be deduced by using the instantaneous reactive power theory [25]. So, the instantaneous active power (p) and the instantaneous reactive power (q) can be expressed as follows [24,26]:

$$p = v_{ac_\alpha} i_\alpha + v_{ac_\beta} i_\beta \tag{3}$$
$$q = v_{ac_\beta} i_\alpha - v_{ac_\alpha} i_\beta \tag{4}$$

where $v_{ac_\alpha}$, $v_{ac_\beta}$, $i_\alpha$ and $i_\beta$ are the $\alpha\beta$ components of 3-phase voltages and currents, respectively.

### *2.1.3 LCL Filter:*

In addition of guaranteeing a constant power delivery to the 3 phase utility grid, grid-connected renewable agents must obey the regulations of power quality. The maximum total harmonic distortion (THD) for the 3-phase currents must be around 5% [27] according to some normative [14,15], whereas the normative for the low order harmonic

distortions is indeed more restrictive. High-frequency ripples are created in the output of the inverter due to the high frequency commutations of the IGBTs [28], meanwhile the low order harmonics are due to non-linear loads. The best solution for reducing the amplitude of the high-frequency ripples is by using of a LC or a LCL filter in the ac side of the inverter [28,29], meanwhile the amplitude of the low order harmonic must also be attenuated to guarantee a good power quality injection to the utility grid, although this a difficult task except a harmonic-compensator (HC) [17] algorithm is used.

#### *2.1.4 EMI filter:*

In a grid-connected Renewable agent, it is necessary to take into account the harmonic pollution due to the Electromagnetic interference (EMI). The EMI interferences in renewable agents are caused by the semi-conductor electronic devices (IGBTs and Diodes). The PWM technique is usually implemented to reduce the generated harmonics by the high-frequency switching of the IGBTs. An EMI filter is a great help to reduce the electromagnetic interference produced by the IGBTs commutations. There are too many methodologies to design the appropriate EMI filter; some of them are based in trial an error. Novel methodologies are cited in several publications, including [30,31].

### *2.2 Control Subsystem*

#### *2.2.1 Synchronization Algorithm:*

The Synchronization Algorithm for attaining a controllable power factor in the connection must detect the phase angle of the 3-phase utility grid voltages with optimal dynamic response and several studies can be found in [32]. The measured signals of the 3 phase utility grid low voltages are contaminated with harmonics, voltage unbalances, and frequency variations; indeed, the used sensors introduce second order harmonics due to accuracy errors. In addition, the classical dq PLL method for synchronization is very sensible to grid voltage unbalances, which also produce second order harmonics in the dc bus [8]. A solution for this is to add a Positive Sequence Detector (PSD) block, which is based on the symmetrical component method or Fortescue theorem [33], to extract the positive sequence of the 3-phase utility grid voltages. The PSD+dq PLL synchronization algorithm is a good alternative to synchronize the Renewable agent to the 3-phase utility grid, but the PSD block has a discrete filter named S90 [34], which can be sensitive to the variation of the nominal frequency of the utility grid [35], and may lead to the power factor degradation of the inverter-grid connection.

A solution for the frequency and phase detections when voltage unbalances and frequency variations occur in the 3-phase utility grid voltages is described in [36], where a Dual Second Order Generalized Integrator FLL (DSOGI-FLL) is proposed. In this, Clarke transformation [13] for the three phase utility voltages is performed in order to obtain its $\alpha\beta$ voltage components, and a Second Order Generalized Integrator [37] with a Quadrature Signal Generation (SOGI-QSG) is used to obtain the $90^{o}$ shifted version of the $\alpha\beta$ voltages components [36]. The DSOGI-FLL synchronization algorithm has a good dynamic response for the phase and frequency detections when unbalance voltages and frequency variations occur in the utility grid, but a poor

harmonic rejection is attained when low order harmonics close to the fundamental frequency appears in the utility grid [16].

A block diagram of a SOGI-QSG is depicted in Fig. 2, and its transfer functions are described by (5) and (6), respectively.

$$D(s) = \frac{v'}{v}(s) = \frac{k\omega' s}{s^2 + k\omega' s + \omega'^2} \tag{5}$$

$$Q(s) = \frac{qv'}{v}(s) = \frac{k\omega'^2}{s^2 + k\omega' s + \omega'^2} \tag{6}$$

where $\omega'$ is the centre angular frequency of the adaptive filter, $k$ is the gain of the SOGI-QSG and $DQ$ are the quadrature signals [36].

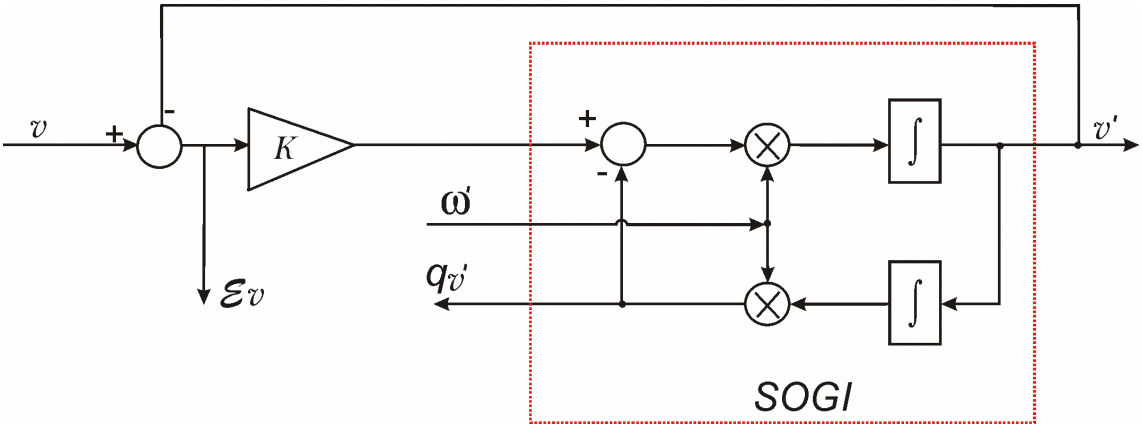


**Fig. 2.** Block diagram of a SOGI-QSG.

Two SOGI-QSG blocks working on the $\alpha\beta$ stationary reference frame are combined to obtain a DSOGI-QSG structure for 3-phase systems [36], shown in Fig. 3.

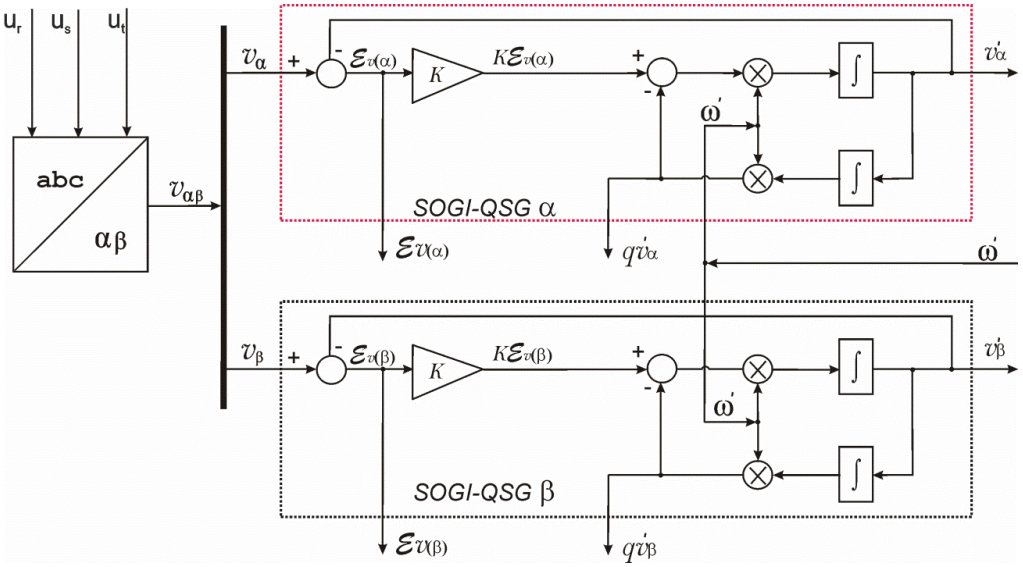


**Fig. 3.** Block diagram of a DSOGI-QSG.

The drawback of the DSOGI-FLL synchronization algorithm regarding harmonic rejection can be overcome by introducing a set of adaptive filters, based on the Quadrature Signal Generation (SOGI-QSG), tuned at different low order harmonic frequencies and working in parallel, together with the Harmonic Decoupling Network (HDN) and the Positive Sequence Calculator (PSC) for each detected harmonic component. This new structure, which is proposed in [16], is named the Multiple Second Order Generalized Integrator Frequency-Locked Loop (MSOGI-FLL) synchronization algorithm. This paper deals with the calculation of the fundamental (1), the second (2), the fifth (5) and the seventh (7) voltage harmonic components, as can be seen in Fig. 4, but the further extension to other harmonic components is completely and easily possible by extrapolation.

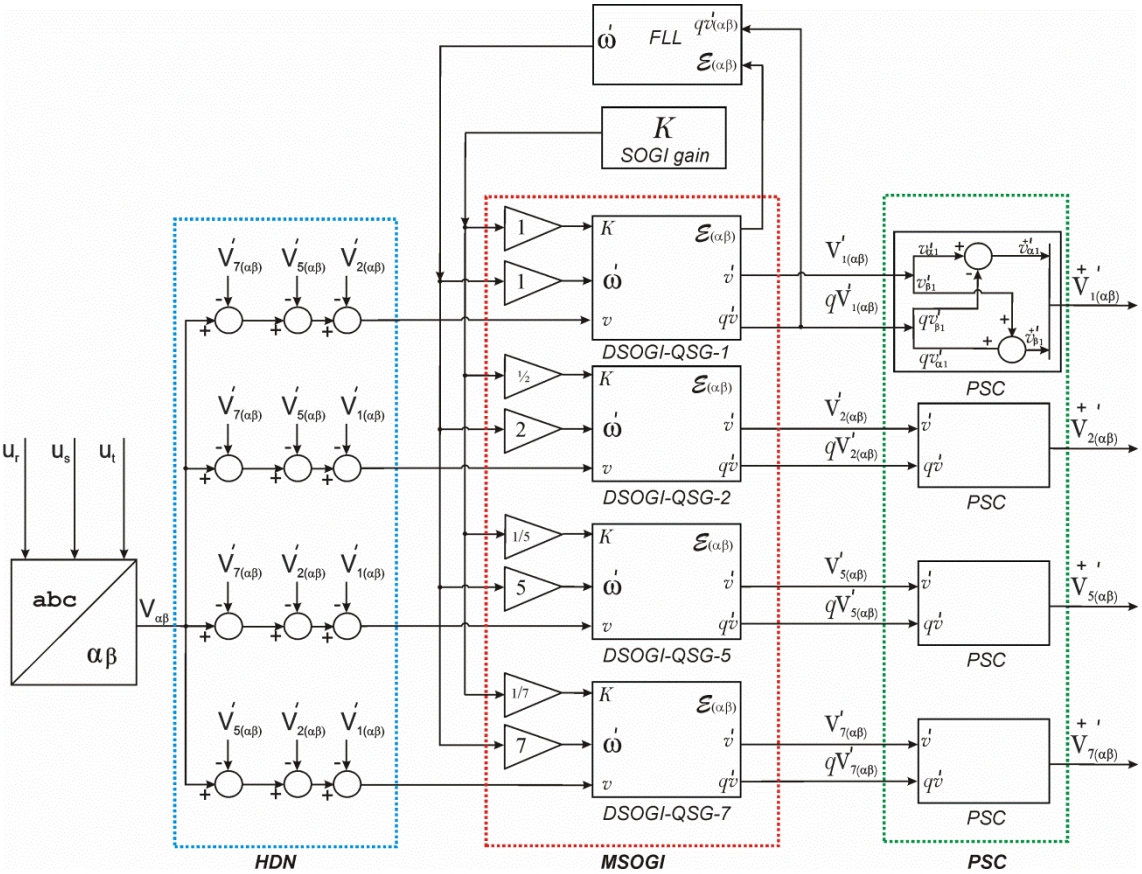


**Fig. 4.** Block diagram of a MSOGI-FLL structure.

The Frequency-Locked Loop (FLL) block is used by the MSOGI-FLL structure above so as to measure the fundamental angular frequency of the input signals $v_{\alpha\beta}$ and is described in detail in Fig. 5: the semi-sum of the product of the error $\varepsilon_v$ and $-qv'$ in each axis is processed by an integrator with gain $-\Gamma$, being $\omega_c$ the feed-forward of the nominal angular frequency for improving its dynamic response. The measured angular frequency $\omega'$ is used to set the frequency of each DSOGI-QSG$_i$ block (shown in the red area of Fig. 4) for the voltage harmonic component to be detected [16]. The FLL gain normalization is exerted so as to make this block independent of the gain $k$ of the DSOGI-QSG block and of the amplitude of the utility grid voltage.

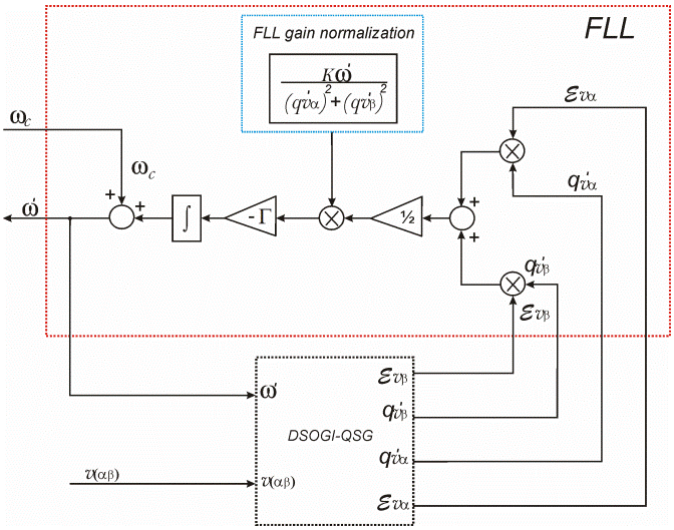


**Fig. 5.** Block diagram of a Frequency-Locked Loop (FLL) with normalized gain used in a DSOGI-FLL.

It must be pointed out that the HDN block (shown in the blue area of Fig. 4) is added to the MSOGI-FLL synchronization algorithm in order to decouple the effect of the several utility grid low order harmonics from the one involved in the calculation with its corresponding DSOGI-QSG$_i$ block. The outputs of the HDN block are sent to the DSOGI-QSGs and the decouple action is achieved by the feedback of the corresponding $V'_{k(\alpha\beta)}$ DSOGI-QSG outputs (k≠i) into the HDN block, as can be seen in Fig. 4. As a consequence, the MSOGI-FLL synchronization algorithm is able to detect the separated voltage harmonic components of the 3-phase utility grid voltages.

Knowing that the instantaneous positive sequence component ($v^+_{abc}$) of an unbalanced voltage vector $v_{abc}$ is given by [38]:

$$v^+_{abc} = \left[ v_a^+ \; v_b^+ \; v_c^+ \right]^T = \left[ T_+ \right] v_{abc} \; ; \; \left[ T_+ \right] = \frac{1}{3} \begin{pmatrix} 1 & a & a^2 \\ a^2 & 1 & a \\ a & a^2 & 1 \end{pmatrix} \tag{7}$$

Where:

$$a = e^{j\frac{2\pi}{3}} = -1/2 + e^{j\frac{\pi}{2}}\sqrt{3}/2$$

Performing a Clarke transformation for the 3-phase utility voltages:

$$v_{\alpha\beta} = \left[ T_{\alpha\beta} \right] v_{abc} \; ; \; \left[ T_{\alpha\beta} \right] = \sqrt{\frac{2}{3}} \begin{pmatrix} 1 & -\frac{1}{2} & -\frac{1}{2} \\ 0 & \frac{\sqrt{3}}{2} & -\frac{\sqrt{3}}{2} \end{pmatrix} \tag{8}$$

The instantaneous positive voltage components are giving by:

$$v^+_{\alpha\beta} = \left[ T_{\alpha\beta} \right] v^+_{abc} = \left[ T_{\alpha\beta} \right] \left[ T_+ \right] v_{abc} = \left[ T_{\alpha\beta} \right] \left[ T_+ \right] \left[ T_{\alpha\beta} \right]^T v_{\alpha\beta} = \frac{1}{2} \begin{pmatrix} 1 & -q \\ q & 1 \end{pmatrix} v_{\alpha\beta} \tag{9}$$

where $q = e^{-j\frac{\pi}{2}}$ is a phase-shift operator to obtain the in-quadrature version of an original wave form.

Using Eq. (9), Positive Sequence Calculator (PSC) structures (shown in the green area of Fig. 4) can be used at the output of each DSOGI-QSG block in order to obtain the positive sequence of each harmonic component of the 3-phase utility grid voltages when unbalances occur.

The phase angle of the positive sequence of the fundamental component of the 3-phase utility grid voltages can be calculated as follows:

$$\theta_1^{+'} = \tan^{-1}\left(\frac{V_{1\beta}^{+'}}{V_{1\alpha}^{+'}}\right) \tag{10}$$

### *2.2.2 Maximum Power Point Tracking:*

The Voltage characteristic of a PV module is not lineal and is time-variant due to a series of atmospheric conditions [39]. In grid-connected renewable agents it is necessary to extract the maximum available power to increase the efficiency of the system and a Maximum Power Point Tracking (MPPT) module is used for this. The MPPT is an essential part of a PV system and several methods have been designed [40], among them, Perturbation and Observation (P&O), Incremental conductance (Inc Cond.), and Ripple Correlation Control (RCC) are mostly used [41].

### *2.2.3 Cascaded control*

The control strategy uses a cascaded control, whose block diagram for the small-signal model is shown in Fig. 6. In this, Proportional-Resonant (PR) regulators are used for the inner line currents, whereas a classical Proportional-Integral (PI) regulator is used for the outer dc bus voltage.

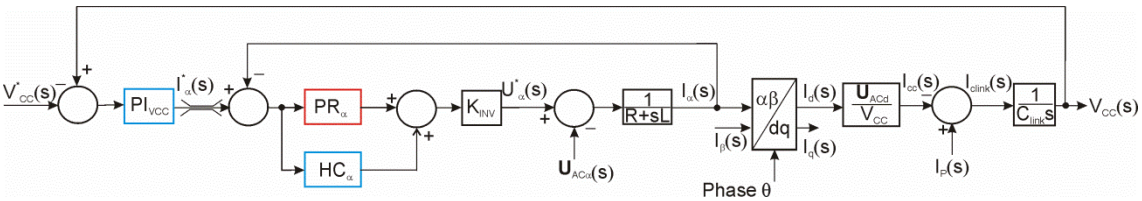


**Fig. 6.** Block diagram of the small-signal model of the cascaded control.

#### *2.2.3.1 Outer loop*

The outer loop regulator compares the dc bus voltage in the link capacitor with the reference which comes from the MPPT algorithm block, keeping a constant dc voltage and assuring the power flow balance between the PV system and the utility grid. This control loop has been performed by using a PI controller and $K_I$ and $K_P$ are calculated under the recommendations in [42,43], neglecting the influence of the faster inner loop, whose transfer function is approximated to unity.

The tuning of the PI controller will define its dynamic response according to the crossover frequency ($f_{cV}$), the phase margin ($PM_V$), and the damping factor ($\zeta_c$) specified for a rated power and the link capacitor ($C_{link}$). Since this paper is mainly focused in the study of PR controllers, the reader interested in more details about this topic can see several scientific references such as [42-47], in which the classical PI behavior is explained in detail.

#### *2.2.3.2 Inner loop*

Classical PI regulators produce zero steady-state error for dc signals due to its integral part. In a similar way, when sinusoidal signals are to be regulated, Proportional-Resonant (PR) regulators must be used for zero steady-state error behaviour instead.

*a) Proportional-Resonant (PR) regulators:*

In the Stationary Refrence Frame Control (PR control), a Clarke transformation (abc->$\alpha\beta$) of the 3-phase line currents is carried out and its sinusoidal $\alpha\beta$ components are obtained. Then, two Proportional-Resonant (PR) controllers are used for both in the inner control loop, allowing the synchronization of the 3-phase inverter line currents with the 3-phase utility grid voltages, and avoiding the non-zero stady-state error if PI controllers were used.

The ideal Proportional-Resonant transfer function is described by (11) wich has an infinite gain at the frequency $\omega_0$ and no gain or phase shift at other frequencies [17]:

$$G_{PR}(s) = K_P + \frac{2K_I s}{s^2 + \omega_0^2} \tag{11}$$

Where $K_P$ is the Proportional gain, $K_I$ is the integral gain, and $\omega_0$ is the resonance angular frequency of the controller.

The ideal PR has an infinite gain within a narrow bandwidth around the resonance frequency $\omega_0$, which may lead to stability and digital implementation problems. Adding the cut-off frequency $\omega_c$, as a new term to (11), leads to a non-ideal PR with finite gain and an improved transient response [17], solving the stability problems and making easier the digital implementation. The transfer function of the non-ideal PR Controller is shown in (12).

$$G_{PR}(s) = K_P + \frac{2K_I \omega_c s}{s^2 + 2\omega_c s + \omega_0^2} \tag{12}$$

The dynamic of the system in terms of bandwidth, phase and gain margin will depend of the proportional gain $K_P$ [48] which is adjusted in a similar way as it is tuned in a PI controller; the stady-state error will depend of the integral gain $K_I$ whose value will be selected comparatively high, but holding the limits for stability [17]. The second term of (12) can be viewed as a Generalized Integrator (GI) [37].

*b) Harmonic Compensation (HC):*

The use of the Proportional-Resonant (PR) controller in the inner current loop opens the possibility of performing a harmonic compensator procedure with minimal computational burden in order to deliver a good power quality to the utility grid. This harmonic compensation is achieved by cascading multiple Genaralized Integrators (GI) which are tunned to resonate at specific low order frequencies [8]. In this paper, as an example of this explanation, the 5th and 7th voltage harmonics will be introduced in the utility grid voltages, meanwhile, a harmonic compensator structure for the 5th and 7th harmonics (shown in Fig.7) will be added to the inner current controller. The transfer function of a harmonic compensator [17] is described by (13).

$$G_h(s) = \sum_{h=5,7} \frac{2K_{ih}\omega_c s}{s^2 + 2\omega_c s + (h\omega_0)^2} \tag{13}$$

where $h$ is the harmonic to be compensated, $\omega_0$ is the fundamental angular frequency and $K_{ih}$ is the integral gain for harmonic $h$.

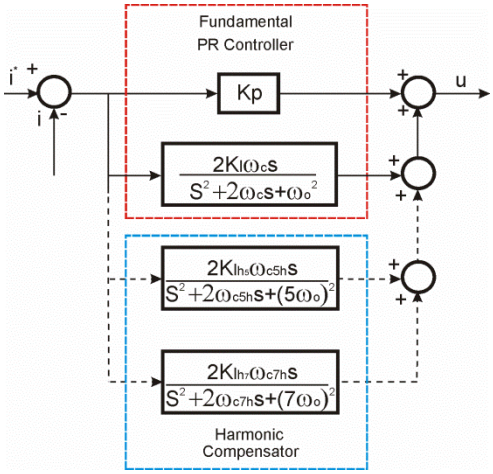


**Fig. 7.** PR Controller + Harmonic Compensator structure.

It must be pointed out that the harmonic compensator HC shown in Fig. 7 does not affect the dynamics of the PR controller, because each filter block will work at its own resonance frequency.

## 3. A Case of Study

The model of the power module includes the 3-phase VSI built with the 6-pack-integrated intelligent Power System *SkiiP 513GD172-3DUL* from *Semikron*, which includes the IGBTs semiconductors for the 3-phase power-poles, and configured to work at 12.208KHz of PWM switching frequency ($F_{PWM}$=12.2kHz (244th harmonic)). The values of the components of the LCL filter, the distribution transformer, and the utility grid are resumed in Table 1 at left, meanwhile at right are the cutoff frequencies and damping factors of the LCL filter.

**Table 1.** Power subsystem characteristics.

| | | |
|---|---|---|
| • R=0.0465Ω<br>• L=1.1mH<br>• C=4μF (Y-connexion)<br>• Transformer:<br>  • $R_t$= 0.247 Ω<br>  • $L_t$= 640 μH, neglecting the magnetizing effect<br>• 3-phase utility grid voltage: 132.8V rms (phase-to-neutral) | $f_c = \frac{1}{2\pi}\frac{R}{L} = 6.72Hz$ | First order RL section |
| | $f_o = \frac{1}{2\pi\sqrt{LC}} = 2400Hz$<br>$(harm = 48)$<br>$\zeta = \frac{\omega_o}{2}RC = 0.0014$ | Second order LC section |
| | $f_{ot} = \frac{1}{2\pi\sqrt{L_t C}} = 3145.6Hz$<br>$(harm = 63)$<br>$\zeta_t = \frac{\omega_o}{2}R_t C = 0.0098$ | Second order LtC section |

The parameters for the Control Subsystem and the MSOGI-FLL Synchronization Algorithm are resumed in Table 2.

**Table 2.** Control Subsystem and Synchronization Algorithm characteristics.

- $K_{INV}$=400V ($V_{CC}$=600V)
- $C_{link}$=2300μF ($\Delta V_{CCmáx}$=60V)
- $f_{cI}$=1220.8Hz, crossover frequency for the inner current loop
- $PM_I$=63.5°
- $K_P$ =0.019
- $K_I$ =10
- $K_{Ih5} = K_{Ih7}$ = 10
- $\omega_0$ = 314.16rad/s
- $\omega_c$ =1rad/s
- $\omega_{c5h}$ =1rad/s, fifth harmonic
- $\omega_{c7h}$ =1rad/s, seventh harmonic
- $f_{cV}$=12.2Hz, crossover frequency for the outer dc bus voltage loop
- $PM_V = PM_I$
- $\zeta_c = \sqrt{2}/2$
- ΔI=16.7A (S=10KVA)
- $u_{ACd}$=132.8V

**MSOGI-FLL parameters**

- $k$ =1.41, gain of the DSOGI-QSG blocks
- Γ =200, gain to set the FLL settling time

A bode plot of (11) is shown in Fig. 8 for $K_P$ = 0.019, $\omega_0$ = 314.16rad/s and $K_I$ = 10. It can be seen the very high gain around $\omega_0$.

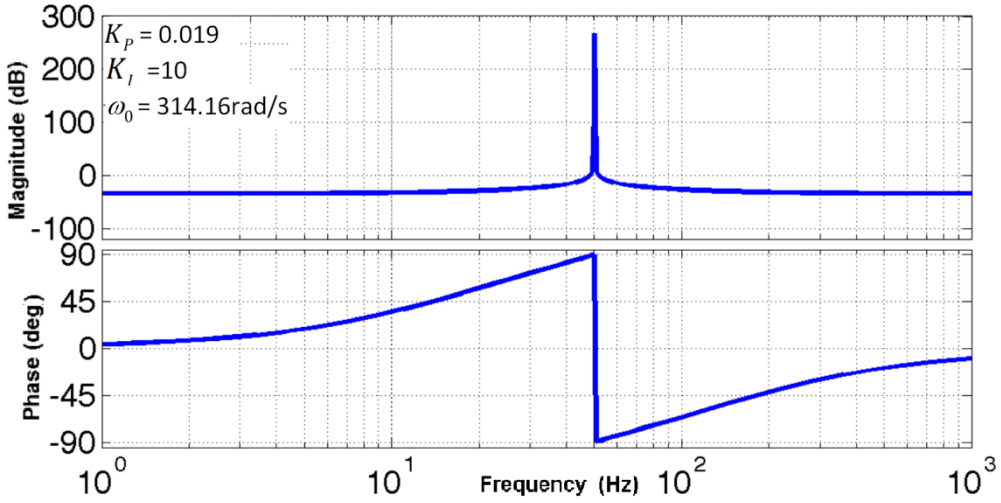


**Fig. 8.** Bode plot of an ideal PR controller.

In order to assure a good transient response with minimum steady-state error, an adequate cut-off frequency $\omega_c$ must be chosen for the non-ideal PR controller. For this, several Bode plots of (12) are shown in Fig. 9a for $K_P$ = 0.019, $\omega_0$ = 314.16rad/s, $K_I$ =10 and $\omega_c$ =1rad/s, 10rad/s and 20rad/s. The upper zone of Fig. 9a shows that finite gain is achieved for all $\omega_c$, meanwhile the increment of $\omega_c$ increases the bandwidth which can help to obtain a certain tolerance in order to support a small variation of the nominal frequency, but at the same time, avoiding the negative influence of the low order harmonics not involved in the PR controller behaviour if a high value of $\omega_c$ were used. Then, $\omega_c$ =1rad/s is chosen because the resonant filter will be more selective in frequency with a high harmonic rejection rate, as can be observed in the trace in red of Fig. 9a.

Adding the effect of the Harmonic Compensator (trace in red) described in (13), to the PR controller (trace in blue) described in (12), an extension of the previous analysis can be done for the influence of the low order harmonics of the 3-phase utility grid voltages. In addition, the dynamic of the inner current loop (block diagram described in Fig. 6 and parameters in Tables 1 and 2) can be studied by taking into account the behaviour of its open loop Bode depicted in Fig. 9b, in which $PM_I$=63.5º and a crossover frequency $f_{cI}$=1220.8Hz is set. The harmonic compensation is carried out by the effect of the resonant filters at $5f_0$ = 250Hz, and $7f_0$ =350Hz.

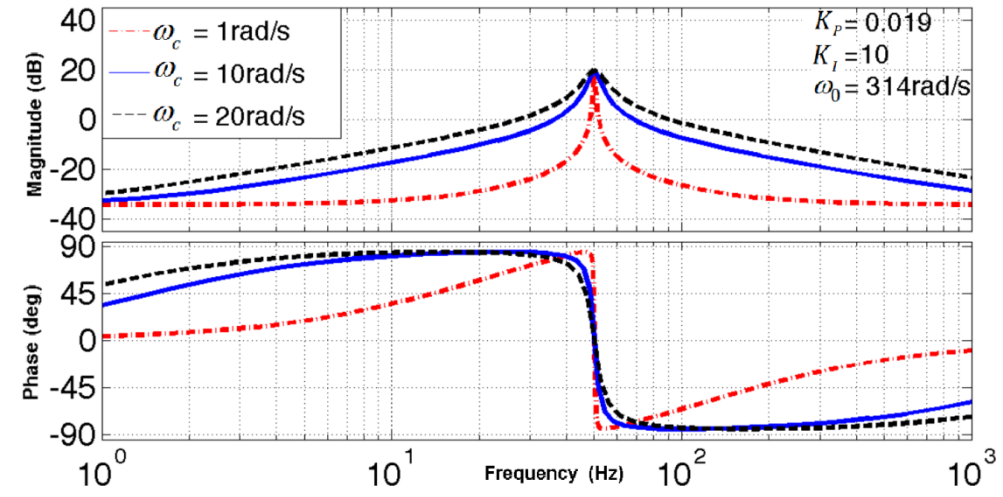


(a)

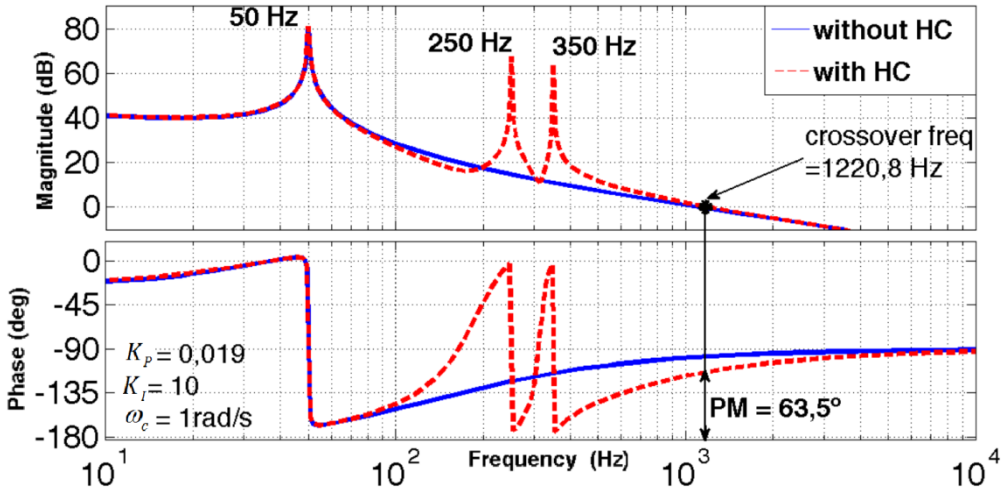


(b)

**Fig. 9.** a) Bode plot of non-ideal PR controller using several values for $\omega_c$.
b) Open loop Bode plot of the PR Controller + Harmonic Compensator + Plant.

## 4. Simulations

Some simulations in MATLAB/SIMULINK environment are shown to validate the operation of the PV Generator grid-connected system using the parameters of the Power and Control Subsystems shown in Table 1 and 2, respectively. Figure 10a shows the SIMULINK model of the proposed system, where a discrete model is used for the Plant with a sample time of 2.56μs. The controller block includes the MSOGI-FLL synchronization algorithm and the cascaded control exerted. The SIMULINK implementation of the cascaded control used in this paper is shown in Fig. 10b.

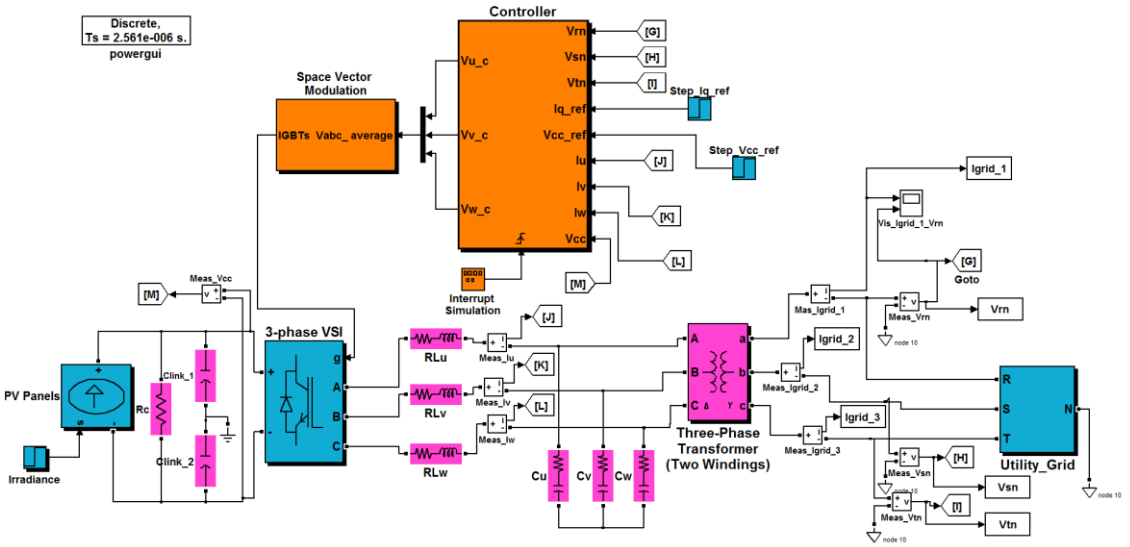


(a)

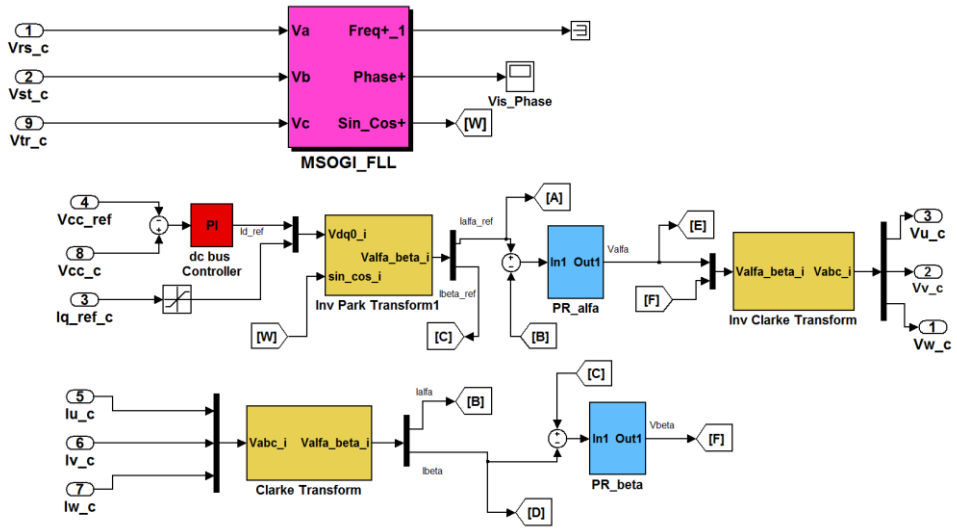


(b)

**Fig. 10.** a) SIMULINK model of the PV Generator grid-connected system.
b) SIMULINK implementation of the cascaded control.

In order to simulate the response of the 3-phase grid-connected VSI to different input conditions, some time simulations are shown in Fig. 11, 12, 13.

The time response to a change in the MPPT of the I-V curve of the PV Generator, is simulated with a corresponding step in the dc bus voltage reference $V^*_{CC}$ at 1s. Holding a constant incoming output current from the PV Generator for a specific irradiance, a step from 500V to nominal value (600V) is exerted at 1s as can be seen in Fig. 11: the proper time response of the dc bus voltage regulator is shown in blue.

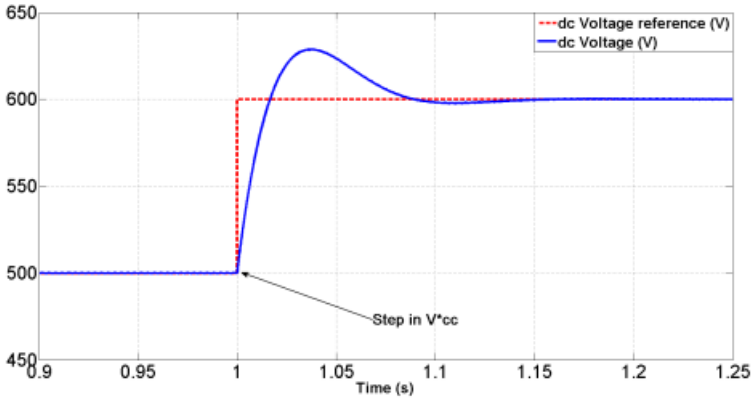


**Fig. 11.** Time evolution of the dc bus voltage for a step in $V^*_{CC}$ with constant output current in PV Generator.

Figure 12 shows the time simulation of a variation in the incoming irradiance. For this, a step in the output current of the PV Generator is exerted at 1s from a 50% up to nominal conditions with constant dc bus voltage reference ($V^*_{CC}$): in this case, the time evolution of the utility grid voltage and current at phase 1 is depicted at left side, meanwhile the instantaneous active power increases from 5kW to 10kW (trace in red), as it is shown at the right side of the Figure, and the instantaneous reactive power is almost constant (trace in blue).

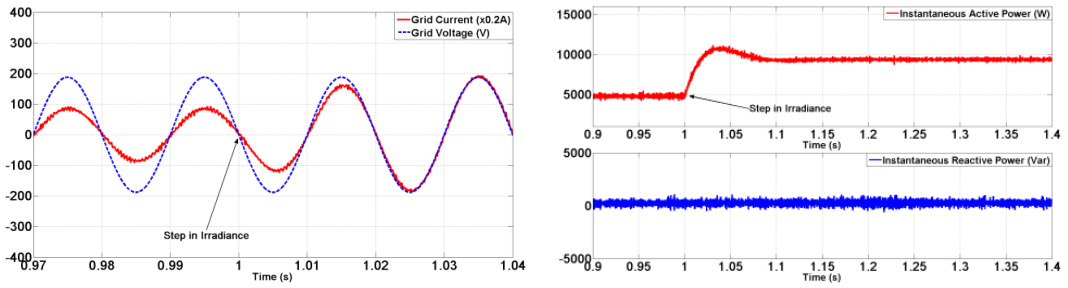


(a) (b)

**Fig. 12.** Time simulations for a step in irradiance with a constant dc bus voltage.
**a)** Time evolution of the utility grid voltage and current at phase 1.
**b)** Time evolution of the instantaneous active and reactive powers.

An important aspect in grid-connected renewable agents is to select a suitable power factor according to the grid demand (active or reactive power) [49]. For this, a time simulation of the power factor control is depicted in Fig. 13: the time evolution of the utility grid voltage and current at phase 1 is displayed at left side. Prior 1s, the grid voltage and current are synchronized in phase and frequency for unitary power factor operation; a drop step in the reference reactive power current is exerted at 1s (from zero to -33.22A), with constant output current at the PV Generator and the dc bus voltage, and the unitary power factor operation is not achieved in this condition (the utility grid current lags the grid voltage). In can be observed the response of the power subsystem with the corresponding step of 4.4kVar in the instantaneous reactive power at the right side of the Figure (trace in blue), meanwhile the instantaneous active power is almost constant around 10kW (trace in red) due to the decoupled control exerted.

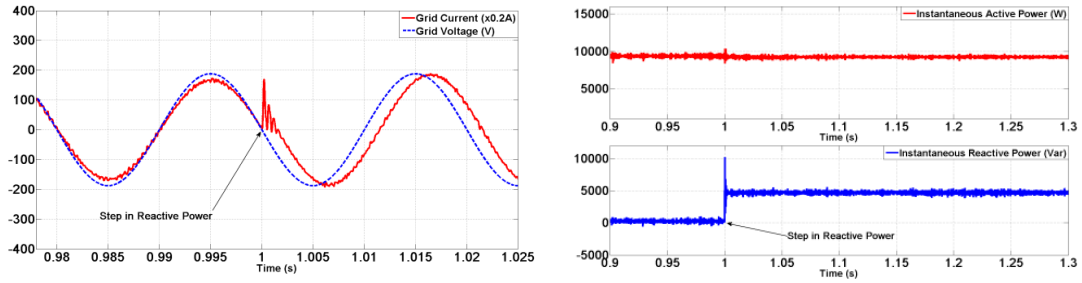


(a) (b)

**Fig. 13.** Time simulations for a step in reactive power with constant output current at the PV Generator and constant dc bus voltage.
a) Time evolution of the utility grid voltage and current at phase 1.
b) Time evolution of the instantaneous active and reactive powers.

In Fig. 14, the 5$^{th}$ and 7$^{th}$ harmonics are introduced in the low voltage 3-phase utility grid with a distortion in its amplitude of 50% for both. In Fig. 14a no harmonic compensation is performed, and then, the time evolution of the utility grid current at phase 1 is distorted due to the harmonic pollution. On the other hand, the time evolution of the grid current at phase 1 is shown in Fig.14b when the harmonic compensator structure shown in Section 2 is used. For the latter, a perfect sine-wave grid current without harmonic pollution is observed.

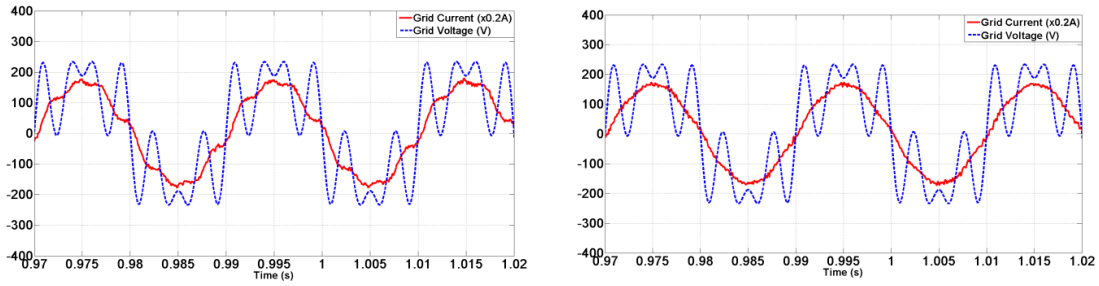


(a) (b)

**Fig. 14.** Utility grid voltage and current at phase 1. The grid voltage is distorted in amplitude by 50% for the 5$^{th}$ and 7$^{th}$ harmonics
a) No Harmonic compensation.
b) Harmonic compensation.

## 5. Experiments using RTDS

In order to validate the control algorithms, some experiments are carried out in this Section using a DS1006 DSPACE platform with several I/O and DAC blocks, the DS5202 Electric Motor HIL Solution boards, and an oscilloscope for parameters monitoring. A photo of the Real-Time Digital Simulation Platform is shown in Fig.15 and the configuration setup is shown in Fig.16. The model blocks of the control and power subsystems are built in MATLAB/SIMULINK Inc., the C-code is generated with Real-Time Workshop from SIMULINK and downloaded into the DSPACE platform.

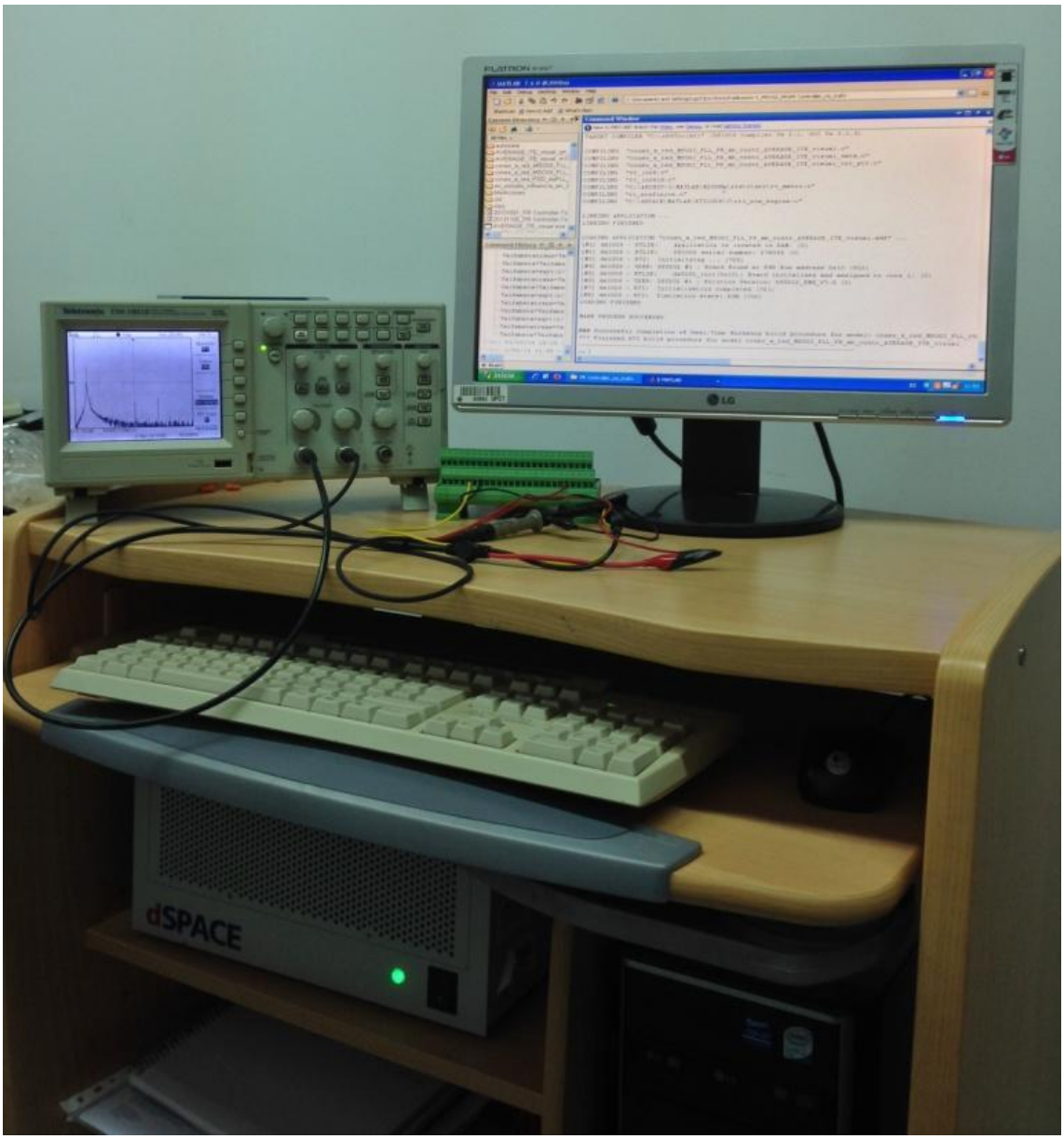


**Fig.15.** Photo of the DSPACE platform for RTDS.

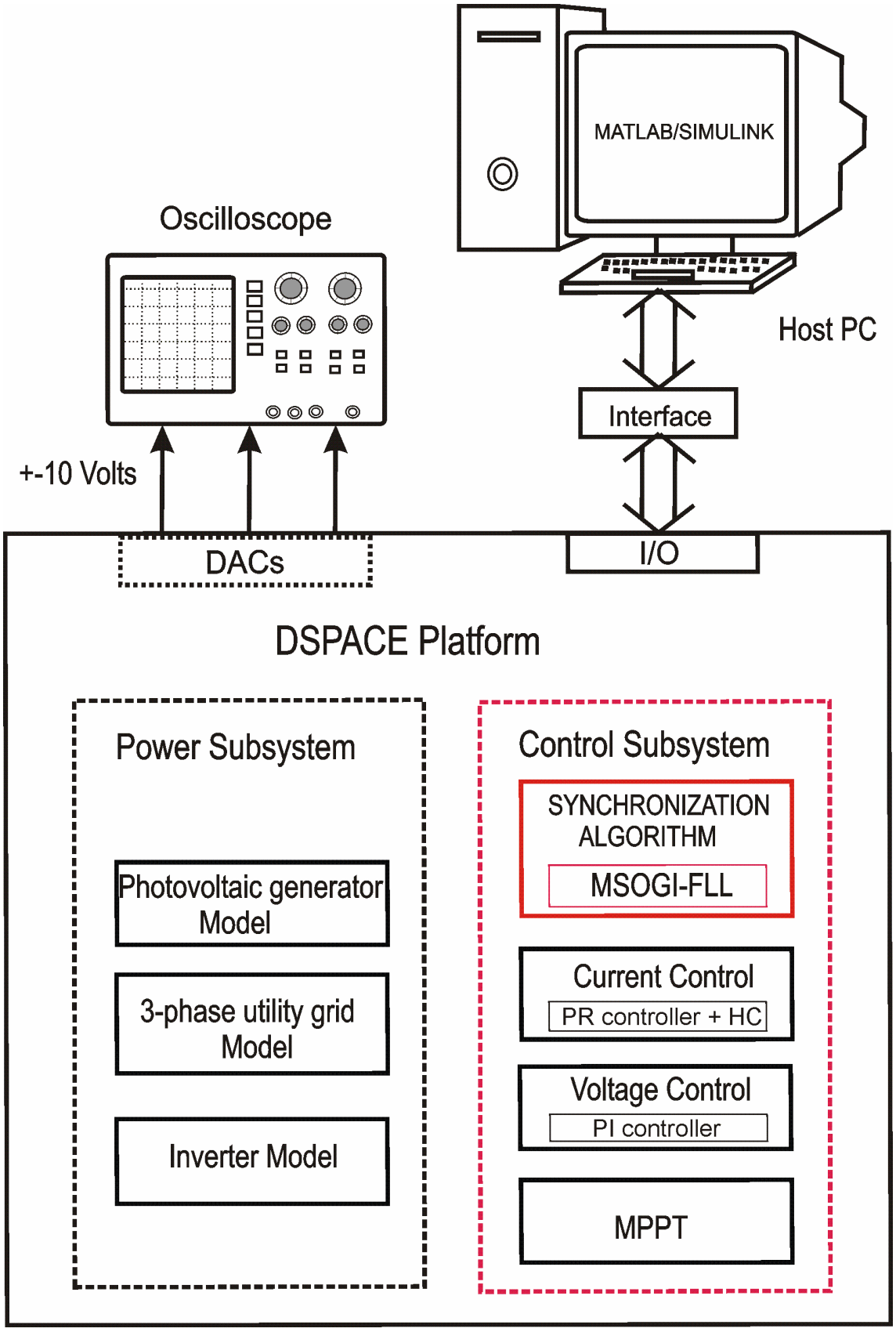


**Fig.16.** Configuration of the DSPACE platform for the real-time testing using a host PC, a DS1006 DSPACE board with a digital to analog converter interface and an oscilloscope for parameters monitoring.

Figure 17a shows the real-time evolution of dc bus voltage when a step in the reference $V^*_{CC}$ from 500V to 600V is exerted, showing a good dynamic response of the outer dc bus regulator loop. The real-time behavior of the instantaneous active power during a variation in the incoming irradiance from a 50% to nominal conditions with constant dc bus voltage is shown in Fig. 17b: in this case, the instantaneous active power increases from 5kW to 10kW approximately.

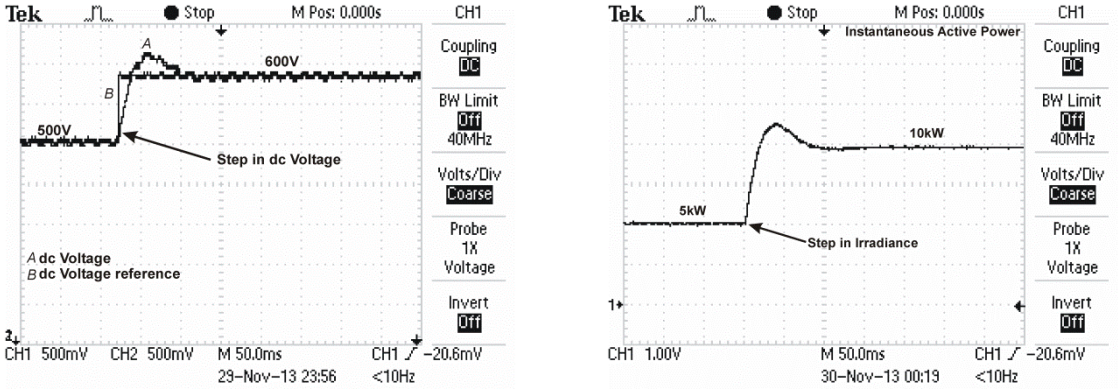


(a) (b)

**Fig. 17.** a) dc voltage bus when a step in $V^*_{CC}$ from 500V to 600V occur.
b) Instantaneous Active power during step of irradiance from 50% to nominal conditions.

Figure 18a depicts the real-time evolution of the instantaneous active and reactive powers at steady state, injecting 10kW and 4.4kVar into the 3-phase utility grid, respectively. In addition, the real-time evolution of the voltage and grid current at phase 1 is shown in Fig. 18b for the same situation: after the reactive step there is a lag of the current yielding a decrement of the power factor of the inverter-grid connection from 1 to 0.92.

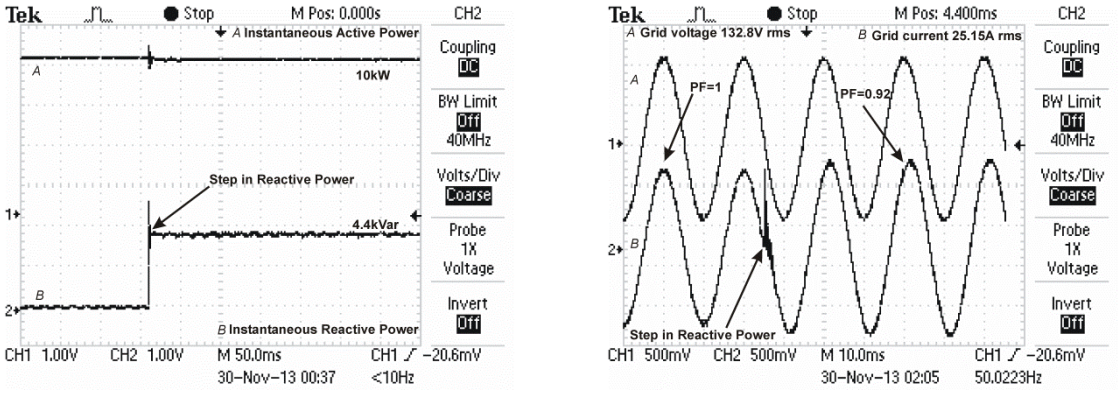


(a) (b)

**Fig. 18.** a) Real-time evolution of the instantaneous active and reactive powers during a step in reactive power.
b) Real-time evolution of the voltage and grid current at phase 1.

In order to show the response of the MSOGI-FLL synchronization algorithm when disturbances occur in the low voltage 3-phase utility grid, Fig. 19 shows the real-time phase and frequency detection obtained by the MSOGI-FLL when harmonic distortion of 50% in the amplitude of the 5$^{th}$ and 7$^{th}$ voltage harmonics are present in the 3-phase utility grid voltages, as well as voltage unbalances (modelled as $V_{\_r}$=187.8$V_{peak}$ $V_{\_s}$=81.64$V_{peak}$ $V_{\_t}$=8.16$V_{peak}$). It must be observed almost a perfect phase and frequency detection attained.

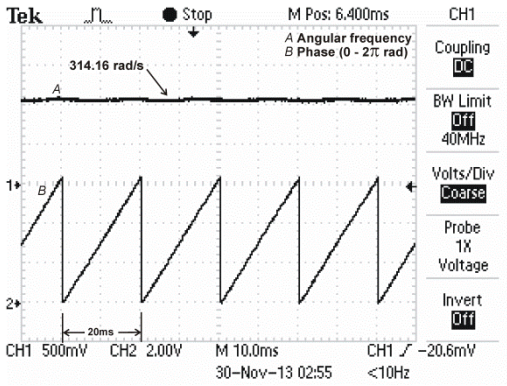


**Fig. 19.** Real-time frequency and phase detection by the MSOGI-FLL.

Figure 20a displays the real-time evolution of the utility grid voltage and current at phase 1: the 3-phase utility grid voltages are affected by 50% pollution in the magnitude of the low order $5^{th}$ and $7^{th}$ harmonics, and no harmonic compensator is used. The frequency spectrum of the grid current at phase 1 is displayed in Fig. 20b, where the fundamental component has a gain of 62dB, meanwhile the $5^{th}$ and $7^{th}$ harmonics have 39dB (7.94% pollution in the amplitude) and 41dB (11.22% pollution in the amplitude), respectively. In this case, the Total Harmonic Distortion (THD) is 13.64%.

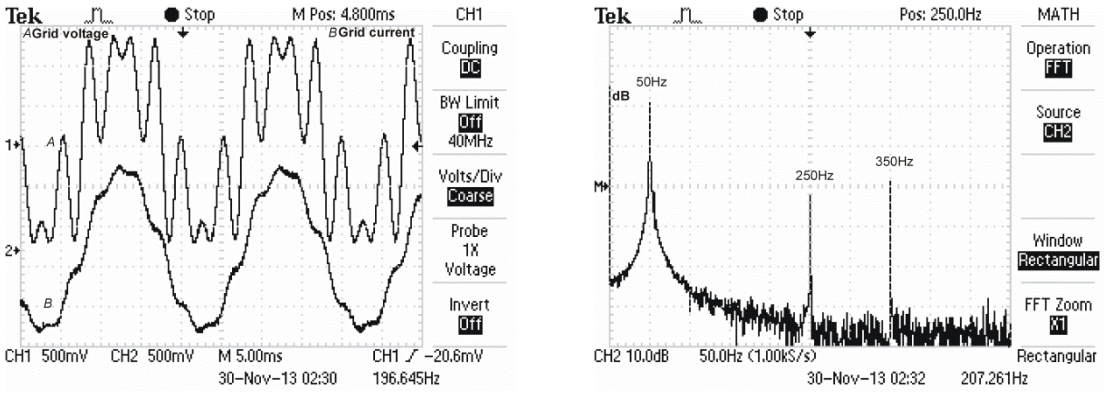


(a) (b)

**Fig. 20.** a) Real-time evolution of the grid voltage (with a 50% pollution in the magnitude of the $5^{th}$ and $7^{th}$ harmonics) and current at phase 1. No harmonic compensator is used.
b) Frequency spectrum of the grid current at phase 1.

On the contrary, Fig. 21a displays the real-time evolution of the utility grid voltage (affected by the same 50% pollution in the magnitude of the low order $5^{th}$ and $7^{th}$ harmonics) and current at phase 1, but a harmonic compensation is performed. The frequency spectrum of the utility grid current at phase 1 is shown in Fig. 21b: the fundamental frequency of the current at phase 1 (50Hz) has a magnitude of 62dB, and the $5^{th}$ and $7^{th}$ harmonics have a magnitude of 28dB (2.51% pollution in the amplitude) and 32dB (3.97% pollution in the amplitude), respectively, yielding a THD=4.69%. In this case, it must be pointed out that an important attenuation of the harmonic contamination is attained when using the harmonic compensator.

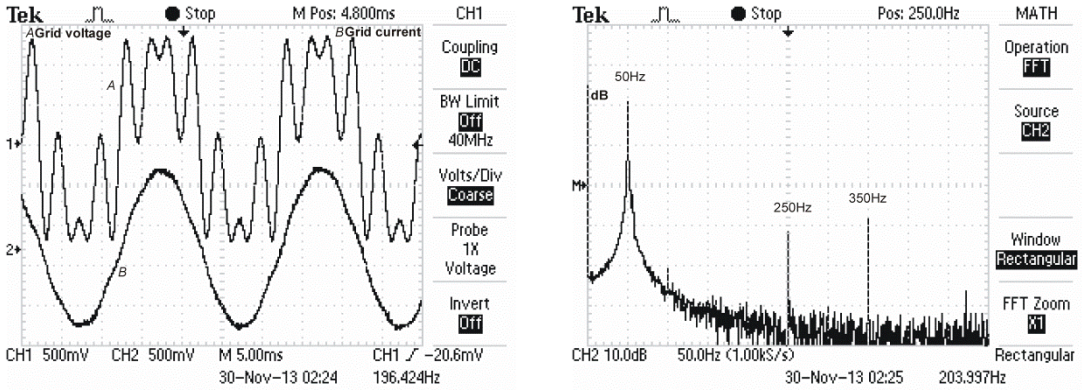


(a) (b)

**Fig. 21.** a) Real-time evolution of the grid voltage (with a 50% pollution in the magnitude of the 5th and 7th harmonics) and current at phase 1. A Harmonic compensator structure is used.
b) Frequency spectrum of the grid current at phase 1.

A summary of the distortions in the amplitude of 5th and 7th harmonics in the grid current at phase 1, the total harmonic distortion, as well as the comparison with the normative [14] is shown in Table 3.

**Table 3.** Harmonic Distortions of the grid current at phase 1.

| Odd harmonics | Grid Current Distortion (not using Harmonic Compensator) | Distortion using Harmonic Compensator | Distortion limit |
|---|---|---|---|
| 5th | 7.94% | 2.51% | < **4.0%** |
| 7th | 11.22% | 3.97% | < **4.0%** |
| | | | |
| | $THD_I$ | $THD_I$ | $THD_I$ limit |
| | 13.64% | 4.69% | < **5.0%** |

## 6. Conclusions

In this paper the Power and Control Subsystems of a Photovoltaic grid-connected agent in a DG scenario was modeled and studied using simulation techniques and experimental tests in a Real-Time Digital Simulator Platform. The main objective was to study the behavior of the control algorithms and its influence in the power quality of the energy fed to the polluted utility grid.

The behavior of the MSOGI-FLL Synchronization Algorithm demonstrates its capability for detecting the positive sequence of the 3-phase utility grid voltages, as well as its excellent capability in the rejection of the low-order harmonic contamination, producing almost an ideal frequency and phase signals, which is an outstanding feature for monitoring and control purposes.

The Proportional-Resonant controller was used to control the line currents of a Voltage Source Inverter which acts as power conditioner between the PV renewable agent and the low voltage 3-phase utility grid. The PR controller structure was also studied and explained in depth, including the Harmonic Compensator structure for reducing the grid currents harmonic contamination when dealing with a distorted utility grid.

The experimental tests carried out for the MSOGI-FLL Synchronization Algorithm, the PR Controller and the Harmonic Compensator structure, using a Real-Time Digital Simulation (RTDS) platform, reinforced the final validation of the control algorithms for the modelled grid-connected renewable agent, allowing a good Power Quality of the Energy fed to the utility grid, as well as the possibility of good performances when unbalances occur.

## Acknowledgements

This work has been supported by a grant from La Fundación Séneca, Agencia de Ciencia y Tecnología de la Región de Murcia, as a part of the Project Ref.11948/PI/09, entitled “Design and construction of a hardware/software prototype for the synchronization and monitoring of renewable agents in a Distributed Generation System” (A. B. Rey-Boué), and a scholarship towards the PhD degree from the Universidad Politecnica de Cartagena with the financing of the Santander Bank (N. F. Guerrero-Rodríguez).

## References

[1] United Nations Framework Convention on Climate Change, Kyoto Protocol. 2005. Available Online at http:unfccc.int/2860.php.

[2] International Energy Agency, IEA Renewables Information Technical report. 2010 Paris.

[3] F.Blaabjerg, C.Zhe, and S.B.Kjaer, Power electronics as efficient interface in dispersed power generation systems, IEEE Transactions on Power Electronics, 19 (2004) 1184-1194.

[4] M.Díez-Mediavilla, C.Alonso-Tristán, M.C.Rodríguez-Amigo, T.García-Calderón, and M.I.Dieste-Velasco, Performance analysis of PV plants: Optimization for improving profitability, Energy Conversion and Management, 57 (2012) 17-23.

[5] Syafaruddin, E.Karatepe, and T.Hiyama, Performance enhancement of photovoltaic array through string and central based MPPT system under non-uniform irradiance conditions, Energy Conversion and Management, 62 (2012) 131-140.

[6] F.Akel, T.Ghennam, E.M.Berkouk, and M.Laour, An improved sensorless decoupled power control scheme of grid connected variable speed wind turbine generator, Energy Conversion and Management, 78 (2014) 584-594.

[7] I.Vechiu, H.Camblong, G.Tapia, and O.Curea, Control of four leg inverter for hybrid power system applications with unbalanced load, Energy Conversion and Management, 48 (2007) 2119-2128.

[8] F.Blaabjerg, R.Teodorescu, M.Liserre, and A.V.Timbus, Overview of Control and Grid Synchronization for Distributed Power Generation Systems, IEEE Transactions on Industrial Electronics, 53 (2006) 1398-1409.

[9] T.Ohnishi, M Hojo, and N.Matsui, Instantaneous line voltage controlled harmonics compensator. IECON. Industrial Electronics Society 2, 754-759. 2000.

[10] T.Ohnishi and M.Hojo, Harmonics compensator by connecting sinusoidal voltage PWM converters. Power Conversion Conference. 3, 1399-1404. 2002.

[11] P.Mattavelli, A closed-loop selective harmonic compensation for active filters, IEEE Transactions on Industry Applications, 37 (2001) 81-89.

[12] M.J.Newman, D.N.Zmood, and D.G.Holmes, Stationary frame harmonic reference generation for active filter systems, IEEE Transactions on Industry Applications, 38 (2002) 1591-1599.

[13] E.Clarke, Circuit Analysis of AC Power Systems, vol. I, Wiley, 1950.

[14] Recommended Practices and Requirements of Harmonic Control in Electrical Power Systems. Standard ANSI/IEEE 519-1992. 1992.

[15] Standard for Interconnecting Distributed Resources with Electric Power Systems, 2003.

[16] P.Rodriguez, A.Luna, M.Ciobotaru, R.Teodorescu, and F.Blaabjerg, Multiresonant Frequency-Locked Loop for Grid Synchronization of Power Converters Under Distorted Grid Conditions, IEEE Transactions on Industry Electronics, 58 (2011) 127-138.

[17] R.Teodorescu, F.Blaabjerg, M.Liserre, and PC.Loh, Proportional-resonant controllers and filters for grid-connected voltage-source converters, IEE Procedings Electric Power Applications, 153 (2006) 750-762.

[18] MATLAB/SIMULINK. The MathWorks, Inc. <http://www.mathworks.com/>. 2008.

[19] L.Freris and D.Infield, Renewable Energy in Power Systems, John Wiley & Sons, Ltd, Publication, United Kingdom , 2008.

[20] M.H.Vishkasougheh and B.Tunaboylu, Simulation of high efficiency silicon solar cells with a hetero-junction microcrystalline intrinsic thin layer, Energy Conversion and Management, 72 (2013) 141-146.

[21] F.Khan, S.Baek, Y.Park, and J.H.Kim, Extraction of diode parameters of silicon solar cells under high illumination conditions, Energy Conversion and Management, 76 (2013) 421-429.

[22] K.W.Böer, Cadmium sulfide enhances solar cell efficiency, Energy Conversion and Management, 52 (2011) 426-430.

[23] K.Zhou and D.Wang, Relationship between space-vector modulation and three-phase carrier-based PWM: a comprehensive analysis [three-phase inverters], IEEE Transactions on Industrial Electronics, 49 (2002) 186-196.

[24] MP.Kazmierkowski, R.Krishnan, and F.Blaabjerg, Control in Power Electronics, Selected Problems, 2002.

[25] H.Akagi, Y.Kanazawa, and A.Nabae, Instantaneous Reactive Power Compensators Comprising Switching Devices without Energy Storage Components. IEEE Transactions on Industry Applications IA-20[3], 625-630. 1984.

[26] H.Akagi, E.Hirokazu Watanabe, and M.Aredes, Instantaneous Power Theory and Applications to Power Conditioning, John Wiley & Sons, 2007.

[27] R.Ekstrom and M.Leijon, Lower order grid current harmonics for a voltage-source inverter connected to a distorted grid, Electric Power Systems Research, 106 (2014) 226-231.

[28] E.J.Bueno, F.Espinosa, F.J.Rodriguez, J.Urefi, and S.Cobrece, Current control of voltage source converters connected to the grid through an LCL-filter, Power Electronics Specialists Conference, 2004 IEEE 35th Annual, 1 (2004) 68-73.

[29] N.Altin and I.Sefa, dSPACE based adaptive neuro-fuzzy controller of grid interactive inverter, Energy Conversion and Management, 56 (2012) 130-139.

[30] D.Hamza, Q.Mei, and P.K.Jain, Implementation of an EMI active filter in grid-tied PV micro-inverter controller and stability verification. IECON. 477-482. 25-10-2012.

[31] C.Po-Shen and L.Yen-Shin, Effective EMI Filter Design Method for Three-Phase Inverter Based Upon Software Noise Separation, IEEE Transactions on Power Electronics, 25 (2010) 2797-2806.

[32] A.V.Timbus, M.Liserre, R.Teodorescu, and F.Blaabjerg, Synchronization methods for three phase distributed power generation systems - An overview and evaluation. Power Electronics Specialists Conference. 2474-2481. 16-6-2005.

[33] C.L.Fortescue, Method of Symmetrical Co-Ordinates Applied to the Solution of Polyphase Networks, American Institute of Electrical Engineers, XXXVII (1918) 1027-1140.

[34] M.Karimi-Ghartemani and M.R.Iravani, A method for synchronization of power electronic converters in polluted and variable-frequency environments, IEEE Transactions on Power Systems, 19 (2004) 1263-1270.

[35] P.Rodriguez, R.Teodorescu, I.Candela, A.V.Timbus, M.Liserre, and F.Blaabjerg, New Positive-sequence Voltage Detector for Grid Synchronization of Power Converters under Faulty Grid Conditions. Power Electronics Specialists Conference, 2006. PESC '06. 37th IEEE. 1-7. 18-6-2006.

[36] P.Rodriguez, A.Luna, M.Ciobotaru, R.Teodorescu, and F.Blaabjerg, Advanced Grid Synchronization System for Power Converters under Unbalanced and Distorted Operating Conditions. IEEE Industrial Electronics, IECON. 5173-5178. 6-11-2006.

[37] Y.Xiaoming, W.Merk, H.Stemmler, and J.Allmeling, Stationary-frame generalized integrators for current control of active power filters with zero steady-state error for current harmonics of concern under unbalanced and distorted operating conditions, IEEE Transactions on Industry Applications, 38 (2002) 523-532.

[38] W.V Lyon, Applications of the method of symmetrical components, McGraw-Hill, New York, 1937.

[39] K.Barra and D.Rahem, Predictive direct power control for photovoltaic grid connected system: An approach based on multilevel converters, Energy Conversion and Management, 78 (2014) 825-834.

[40] O.Guenounou, B.Dahhou, and F.Chabour, Adaptive fuzzy controller based MPPT for photovoltaic systems, Energy Conversion and Management, 78 (2014) 843-850.

[41] A.Messaia, A.Mellitb, A.Massi Pavanc, A.Guessoumd, and H.Mekkia, FPGA-based implementation of a fuzzy controller (MPPT) for photovoltaic module, Energy Conversion and Management, 52 (2011) 2695-2704.

[42] A.B.Rey-Boué, R.García-Valverde, F.Ruz-Vila, and J.M.Torrelo-Ponce, An integrative approach to the design methodology for 3-phase power conditioners in Photovoltaic Grid-Connected systems, Energy Conversion and Management, 56 (2012) 80-95.

[43] S.Buso and P.Mattavelli, Digital Control in Power Electronics, Morgan & Claypool, 2006.

[44] G.Saglam, C.C.Tutum, and S.Kurtulan, A new PI tuning method for an industrial process: A case study from a micro-cogeneration system, Energy Conversion and Management, 67 (2013) 226-239.

[45] J.Wang, N.Tse, and Z.Gao, Synthesis on PI-based pitch controller of large wind turbines generator, Energy Conversion and Management, 52 (2011) 1288-1294.

[46] I.Attoui and A.Omeiri, Modeling, control and fault diagnosis of an isolated wind energy conversion system with a self-excited induction generator subject to electrical faults, Energy Conversion and Management, 82 (2014) 11-26.

[47] A.Masmoudi, L.Krichen, and A.Ouali, Voltage control of a variable speed wind turbine connected to an isolated load: Experimental study, Energy Conversion and Management, 59 (2012) 19-26.

[48] D.N.Zmood and D.G.Holmes, Stationary frame current regulation of PWM inverters with zero steady-state error, IEEE Transactions on Power Electronics, 18 (2003) 814-822.

[49] K.Himoura, K.Ghedamsia, and E.M.Berkoukb, Supervision and control of grid connected PV-Storage systems with the five level diode clamped inverter, Energy Conversion and Management, 77 (2014) 98-107.